A passive inverse filter for Green's function retrieval

Thomas Gallot,[a] Stefan Catheline, Philippe Roux, and Michel Campillo
Institut des Sciences de la Terre (ISTerre) CNRS: UMR5275 IFSTTAR
Université de Savoie Université Joseph Fourier–Grenoble I INSU OSUG IRD: UR219, France
thomas.gallot@gmail.com, stefan.catheline@obs.ujf-grenoble.fr,
philippe.roux@obs.ujf-grenoble.fr, michel.campillo@obs.ujf-grenoble.fr

Abstract: Passive methods for the recovery of Green's functions from ambient noise require strong hypotheses, including isotropic distribution of the noise sources. Very often, this distribution is nonisotropic, which introduces bias in the Green's function reconstruction. To minimize this bias, a spatiotemporal inverse filter is proposed. The method is tested on a directive noise field computed from an experimental active seismic data set. The results indicate that the passive inverse filter allows the manipulation of the spatiotemporal degrees of freedom of a complex wave field, and it can efficiently compensate for the noise wavefield directivity.

PACS numbers: 43.35.Pt, 43.40.Ph, 43.60.Tj [CG]
Date Received: October 3, 2011 **Date Accepted:** October 24, 2011

1. Introduction

Passive imaging methods are based on the extraction of information contained in an ambient background wavefield through reconstructing the Green's function between the sensors. These methods were first developed in the field of helio-seismology[1] and acoustics,[2] and they have seen growing interest in seismology over the last decade.[3–8] Despite remarkable passive imaging results that have been obtained from cross-correlation techniques,[6,9,10] the hypothesis of the homogeneous repartition of sources[11] for exact Green's function reconstruction is rarely achieved. In geophysics, for example, the seismic ambient noise has been shown to be directive[12,13] and most experimental results can suffer from the effects of the nonisotropic illumination of the receiver array. As a consequence, the improper Green's functions estimation can lead to bias in wave-speed estimation, which will impact upon the tomography results.[14,15] Different methods have been proposed to improve the correlation techniques, such as statistical approaches based on source-distribution models[16] or propagation-medium models.[17] Deconvolution methods have also been demonstrated, both theoretically and numerically, to be able to correct part of the bias in the estimated Green's functions.[18–20] Finally, the correlation of the coda of the correlation (C^3) method[21] minimizes the directivity bias by using seismic stations as virtual sources and the multiple scattered part of the wavefield.

The approach proposed in this study is inspired by the spatiotemporal inverse filter[22] that was developed as an improvement of time reversal focusing on the case of a set of controlled active sources.[23] In a passive configuration, so without active sources, the cross correlations can be interpreted as a time-reversal operation through a virtual time-reversal mirror that is made of noise sources.[24,25] Similarly, the principle of the inverse filter can be extended to the passive configuration. With such a passive inverse filter, the spatial distribution of noise sources is made homogeneous, which leads to improved Green's function reconstruction compared to the standard cross correlation.

[a]Author to whom correspondence should be addressed.

2. Inverse filter: Basic principle

The inverse filter method developed by Tanter *et al.*[26] is based on the matrix formalism of the propagation operator **H** between a set of sources and receivers that accounts for all of the propagation effects within the medium at a given frequency ω. For each source–receiver couple (i, j), the impulse responses $h_{ij}(t)$ are measured by recording the impulse response on receiver j for a pulse-like emission from source i. According to linear system theory, the response $r_j(t)$ on a receiver j to a sum of emitted signals $e_i(t)$, $1 \leq i \leq N_s$, is a convolution product between the emissions and the impulse responses $h_{ij}(t)$:

$$r_j(t) = \sum_{i=1}^{N_s} h_{ij}(t) \otimes e_i(t), \qquad 1 \leq j \leq N_r. \tag{1}$$

In the Fourier domain, Eq. (1) yields to the linear relationship between the emission and receiving column vectors, respectively $E(\omega) = [E_i(\omega)]_{1\leq i\leq N_s}$ and $R(\omega) = \left[R_j(\omega)\right]_{1\leq j\leq N_r}$, through the propagation matrix $\mathbf{H}(\omega)$:

$$R(\omega) = \mathbf{H}(\omega) \cdot E(\omega)\,. \tag{2}$$

Each complex $N_r \times N_s$ matrix $\mathbf{H}(\omega)$ is a Fourier component of the propagation operator. The inverse filter approach consists of choosing an objective vector for the receiving vector [Eq. (3)], with zeros everywhere except on j:

$$R_j^{IF} = \{0 \ldots 0\,1\,0 \ldots 0\}\,. \tag{3}$$

This ideal objective vector is reached for the emission of $E_j^{IF} = \mathbf{H}^{-1} \cdot R_j^{IF}$ according to Eq. (2). This objective vector corresponds to a ponctual focusing without any side lobes. In practice, this ideal focusing is bounded by the spatial sampling and the finite dimension of the array. The inversion process of **H** is highly sensitive to these spatial constraints and to the experimental noise. As proposed by Tanter *et al.*,[22] a singular value decomposition of **H** is performed to select singular values above the noise level, and to avoid the inversion of noise components. This inversion is the critical step for the method and requires careful selection of the singular values. The noise-filtered inverse matrix $\tilde{\mathbf{H}}^{-1}$ is used to compute the ideal emission $\tilde{E}_j^{IF} = \tilde{\mathbf{H}}^{-1} \cdot R_j^{IF}$. Then, the focus pattern $\psi_j(\omega)$ that results is given by the substitution of the emission vector in Eq. (2):

$$\psi_j(\omega) = \mathbf{H}\tilde{\mathbf{H}}^{-1} \cdot R_j^{IF}. \tag{4}$$

Finally, an inverse Fourier transform gives $\psi_j(t) = \left[\psi_{jk}(t)\right]_{1\leq k\leq N_r}$. Each component $\psi_{jk}(t)$ corresponds to the optimal temporal signal refocusing on point j observed on receiver k.

3. Application to seismic data

The inverse filter has mainly been applied to data on linear arrays,[27–29] although there is no geometrical restriction for the source or receiving arrays. In this study, the inverse filter is applied to a complex 2D geometry of sources and receivers [Fig. 1(a)]. This specific geometry arises from an active seismic data set,[30] which includes 1600 sources and 1600 receivers spread out every 25 m on a 1 km × 1 km regular grid. This high density of the sources and receivers is a very interesting characteristic of this data set. Using an appropriate set of sources and receivers, these data have already been used to study the dependence of the Green's function retrieval, using cross-correlation methods as a function of the source spatial distribution.[14,15] Here a specific spatial source distribution, with 70% in the top half-space, was chosen to create strong wavefield directivity. During this active seismic survey, the sources (vibrating trucks) were located at

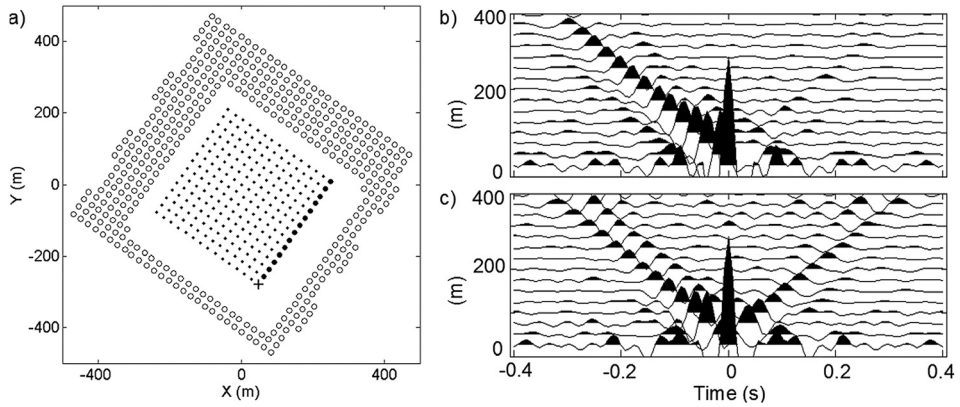

Fig. 1. (a) Experimental geometry of the active seismic data: $N_r = 225$ receivers (points) distributed on a grid of 400×400 m surrounded by $N_s = 386$ sources (circles). The spatial distribution of the sources was chosen to create nonisotropic illumination with 70% of the sources in the top half-space ($Y > 0$). (b) The cross-correlation functions $[C_{1k}(t)]_{1\leq k\leq 15}$ along the receiving line (bold points in a) have a temporal asymmetry due to the spatial repartition of sources. (c) The inverse filter $[\psi_{1k}(t)]_{1\leq k\leq 15}$ provides significant improvement to the temporal symmetry by recovering the diverging waves ($t > 0$ s) coming from the few sources of the bottom half-space.

386 different positions and the 4 s long responses $h_{ij}(t)$ (for source i and receiver j) were recorded on a grid of 15×15 geophones [Fig. 1(a)]. In a 7–25 Hz frequency bandwidth, the wavefield is dominated by surface waves with an average speed of 1000 m/s.

To compare with the inverse filter approach, the classical cross-correlation $C_{jk}(t)$ is first computed between receivers j and k:

$$C_{jk}(t) = \sum_{i=1}^{N_s} h_{ij}(-t) \otimes h_{ik}(t)\,. \tag{5}$$

As often used in seismology, a whitening process is systematically applied to the signals. The cross correlation computed for the line of 15 receivers ($1 \leq k \leq 15$) are displayed as bold points in Fig. 1(a). The focus point $j = 1$ (indicated by a cross) was chosen to reinforce the spatial nonisotropy of the source distribution. The cross-correlation $C_{1k}(t)$ is equivalent to a time-reversal field for a source located at receiver $j = 1$, observed on k, through a mirror constituted by the N_s sources.[24] Consequently, the cross-correlation field, Fig. 1(b), can be interpreted as a time reversal spatiotemporal focusing with a converging wave at negative time, a collapse on the receiver $j = 1$ at $t = 0$, and then a diverging wave at positive time. Coming from the half-space with a high number of sources, converging waves ($t < 0$ s) have larger amplitudes than diverging waves ($t > 0$ s) issued from the half-space with a lower number of sources that barely emerges from the background noise. This temporal asymmetry is observed in many cross-correlation experiments[15] and it can be related to the improper spatial repartition of the sources. In our controlled experiment, the low diverging wave amplitude is thus due to the lack of sources in the bottom half-space.

In a second step, the inverse filter approach is used to focus the wavefield on receiver j, according to the objective vector defined in Eq. (3). The propagation operator $\mathbf{H}$ is constructed from the experimental responses $h_{ij}(t)$, and the singular values are selected for each frequency to construct the noise-filtered matrix $\tilde{\mathbf{H}}^{-1}$. In practice, all of the values that are 5 dB above the noise area are conserved, which represents from 40 to 70 singular values. The noise is characterized by an exponential decrease in the singular values.[22] The field computed from the spatiotemporal inversion $\psi_{1k}(t)$ given by Eq. (4) is represented in Fig. 1(c). The converging and diverging waves have the same amplitudes, as if the spatial distribution of the sources was uniform. The inverse filter can modulate the amplitude of each source according to the receiving objective

vector, which mitigates the lack of sources in the bottom half-space. This preliminary study confirms that even for complex 2D arrays, the focused field can be spatially optimized by the use of the inverse filter approach. As for ultrasonic experiments, the inverse filter method shows better manipulation of the spatiotemporal degrees of freedom for Green's function reconstruction. In the following, this approach is adapted to a passive configuration, where the sources are not controlled anymore.

4. Noise field

In the previous case, each active source was separately recorded on a set of receivers. In contrast, this source control is lost in a noise experiment. Thus, in a passive configuration, a wavefield generated by randomly activated sources is recorded on the receivers. The noise is created by a random activation time that is applied to the set of 386 active sources, as schematized in Fig. 2. For each receiver j, a single long-time signal $s_j(t)$ contains all of the 4 s responses $h_{ij}(t)$. The activation time t_i of each of the 386 sources was governed by a uniform distribution between $t = 0$ and $t = 1300$ s, which yields many superpositions: 30% of each impulse response on average. A 0.2 s minimum delay between two consecutive t_i's provides a constraint for temporal repartition of the intensity. Through this noise construction, the temporal and spatial information of sources is lost. Even if the peaks are still visible in Fig. 2(b), none can be identified for a specific source. Nevertheless, the spatial nonisotropy of the 386 sources is conserved. The cross correlation computed from this wavefield does not show

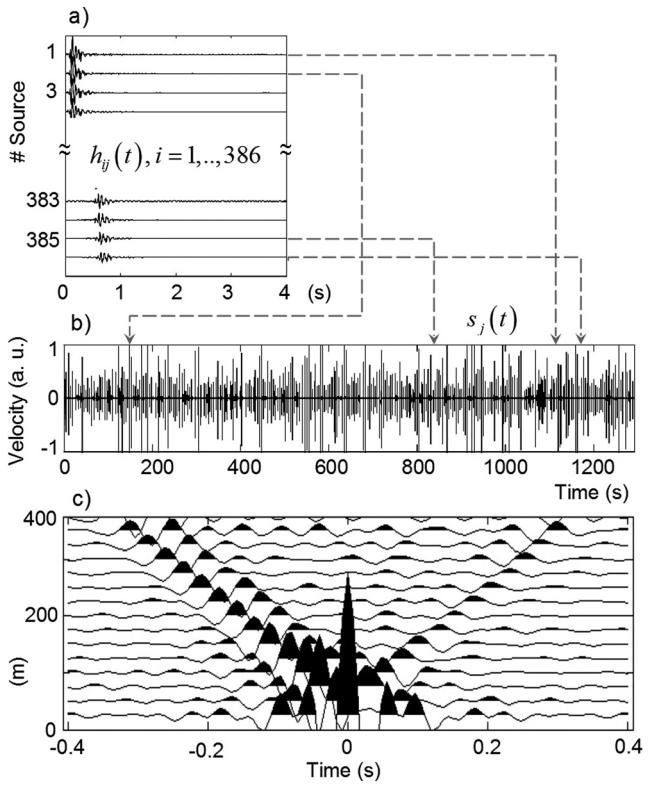

Fig. 2. A noise field is created from the active experimental data set. (a) Each response $h_{ij}(t)$ is randomly inserted into a unique temporal signal $s_j(t)$ (b) with the same random activation time t_i for each receiver j. Spatial and temporal information of the individual sources is lost during this operation, although the global repartition of the sources remains nonisotropic. (c) As in the active case, the response to the passive inverse filter $[\hat{\psi}_{1k}(t)]_{1\leq k\leq 15}$ shows a temporal symmetry that is independent of the spatial source distribution.

significant differences to Fig. 1(b): only the acausal part of the Green's function is well reconstructed. Compared to experimental noise, the use of reconstructed noise has been preferred for two reasons. First, the nonisotropic property of the complex wave field can be controlled through the spatial distribution of active sources, as described in Fig. 1(a). Second, the ideal focus computed by the inverse filter [Fig. 1(c)] provides reference of optimized use of the information available in the wavefield.

5. Passive inverse filter

In a passive configuration, the propagation matrix between sources and receivers is replaced by a noise-like data set recorded on a receiver array. For this goal, the noise $s_j(t)$ on each receiver j is truncated into 6 s long overlapping windows $\hat{h}_{ij}(t)$, $1 \leq i \leq 722$. These parameters were chosen so that, on average, each window contains at least two impulse responses. The basic idea consists of considering each segment as the response to an effective source. This effective source is not an actual point source as each segment is composed of partially overlapping responses of several unknown sources. However, the combination of the responses of these effective sources can be optimized through the inverse filter process. The signals $\hat{h}_{ij}(t)$ constitute, in the Fourier domain, a new propagation operator $\hat{\mathbf{H}}$, which is used for the inverse filter approach, as described in Secs. 2 and 3. As in the active case [Fig. 1(c)], converging and diverging waves of the passive inverse filter refocusing $\hat{\psi}_{jk}(t)$ [Fig. 2(c)] have the same amplitude. In a passive configuration without control of the sources, the inverse filter still played its role, by modulating the amplitude of each effective source, such that the optimal spatial focus can be reached.

So far, the focused field has been observed on a line of receivers in the case of a focus point placed at the bottom of the observation space [Fig. 1(a)], to reinforce the spatial nonisotropy of the source distribution. In the following, the focused fields through correlation and the inverse filter [$C_{jk}(t)$ and $\hat{\psi}_{jk}(t)$] are computed on the whole 15×15 geophone grid. A spatial average is performed with respect to the focal point, which explores all of the grid ($1 \leq j \leq 225$). Two pictures of the spatial and temporal focus were selected before and after the collapse time ($t = 0$). With cross correlation, the amplitude of the converging [Fig. 3(a)] or diverging [Fig. 3(c)] waves clearly reveals

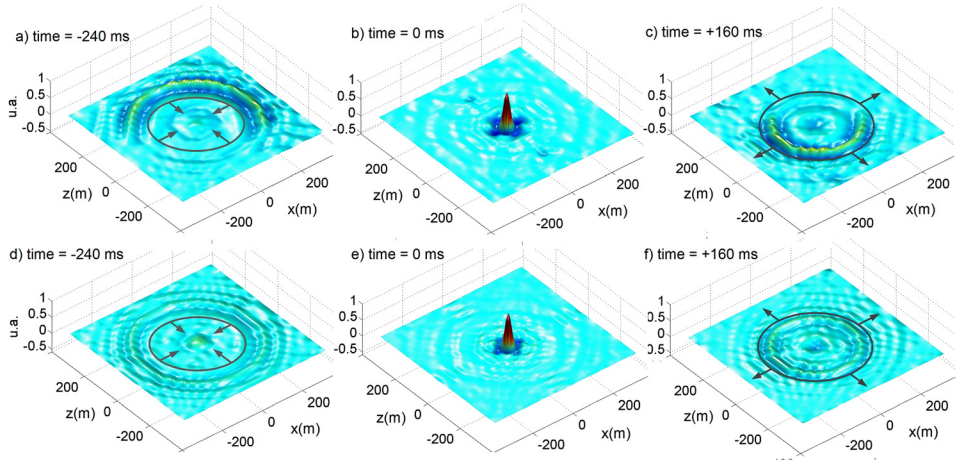

Fig. 3. (Color online) Clichés of Green's function reconstruction from cross-correlation $\langle C_{jk}(t) \rangle_j$ [(a)–(c)] and from the passive spatiotemporal inversion $\langle \hat{\psi}_{jk}(t) \rangle_j$ [(d)–(f)]. The collapse time is taken as the reference $t = 0$ ms. Before ($t = -240$ ms) and after ($t = +160$ ms), the converging and diverging waves are clearly visible. However, the energy distribution is more isotropic with the passive inverse filter and gives a better Green's function reconstruction than with correlation. The arrows indicate the propagation direction.

the spatial distribution of the sources, as most of the intensity before the focus comes from one half-space. However, with the inverse filter approach [Fig. 3(d)–3(f)], the energy distribution is more isotropic: Converging and diverging waves have an almost ideal isotropic distribution of amplitude. The improvement in the Green's function retrieval is possible because of the presence of a few sources in the bottom half-space. Indeed, without any source in the bottom half-space, some spatial frequencies miss in the recorded wavefield and only a biased Green's function would be reconstructed. However, even in this unfavorable case, spatial heterogeneities can act as virtual sources and produce the missing spatial frequencies through scattering. The inverse filter is then only limited by the ability of the measurement device to record the direct wavefield or some scattered wave field component in any direction. Finally, in the case of an anisotropic medium, the inverse filter technique leaves unchanged the anisotropic nature of the medium itself, despite an isotropized spatial distribution of the wavefield intensity.

6. Conclusion

The inverse filter approach is based on the use of a propagation matrix between sources and receivers in order to optimize the spatial and temporal focusing. The improvement in the temporal symmetry of the focus, or as its equivalent, of the Green's functions, computed by the inverse filter is evidence that the wavefield directivity is made homogeneous. The present study demonstrates that the control of sources is not essential for the inverse filter process, and it extends its application to a passive configuration without spatial or temporal information on sources. The ability of the passive inverse filter to be used to extract the unbiased Green's function in the case of a nonisotropic noise field is a promising improvement for passive imaging methods.

Acknowledgments

This work was made possible with the support of Shell. The authors thank the Ministry of Oil and Gas of the Sultanate of Oman and Petroleum Development Oman for permission to use the field data of this study.

References and links

[1]T. L. Duvall, Jr., S. M. Jeffferies, J. W. Harvey, and M. A Pomerantz, "Time-distance helioseismology," Nature (London) **362**, 430–432 (1993).
[2]O. I. Lobkis and R. L. Weaver, "On the emergence of the Green's function in the correlations of a diffuse field," J. Acoust. Soc. Am. **110**, 3011–3017 (2001).
[3]M. Campillo and A. Paul, "Long-range correlations in the diffuse seismic coda," Science **299**, 547–549 (2003).
[4]E. Larose, L. Margerin, A. Derode, B. van Tiggelen, M. Campillo, N. Shapiro, A. Paul, L. Stehly, and M. Tanter, "Correlation of random wavefields: An interdisciplinary review," Geophysics **71**, SI11–SI21 (2006).
[5]P. Roux, K. G. Sabra, P. Gerstoft, W. A. Kuperman and M. C. Fehler, "P-waves from cross-correlation of seismic noise," Geophys. Res. Lett **32**, L19303 (2005).
[6]N. M. Shapiro, M. Campillo, L. Stehly and M. H. Ritzwoller, "High resolution surface-wave tomography from ambient seismic noise," Science **307**, 1615–1618 (2005).
[7]R. Snieder, "Extracting the Green's function from the correlation of coda waves: A derivation based on stationary phase," Phys. Rev. E **69**, 046610 (2004).
[8]K. Wapenaar, "Retrieving the elastodynamic Green's function of an arbitrary inhomogeneous medium by cross correlation," Phys. Rev. Lett. **93**, 254301 (2004).
[9]T. Gallot, S. Catheline, P. Roux, J. Brum, N. Benech, and C. Negreira, "Passive elastography: shear-wave tomography from physiological-noise correlation in soft tissues," IEEE Trans. Ultrason. Ferroelec. Freq. Contr. **58**, 1122 (2011).
[10]K.G. Sabra, P. Gerstoft, P. Roux, W. A. Kuperman, and M. C. Fehler, "Surface wave tomography from microseisms in Southern California," Geophys. Res. Lett. **32**, L14311 (2005).
[11]P. Gouédard, L. Stehly, F. Brenguier, M. Campillo, Y. Colin de Verdiere, E. Larose, L. Margerin, P. Roux, F. J. Sanchez-Sesma, N. M. Shapiro, and R. L. Weaver, "Cross-correlation of random fields: Mathematical approach and applications," Geophys. Prospect. **56**, 375–393 (2008).

[12]P. Roux, "Passive seismic imaging with directive ambient noise: Application to surface waves and the San Andreas Fault in Parkfield, CA," Geophys. J. Int. **179**, 367–373 (2009).
[13]L. Stehly, N. Shapiro, and M. Campillo, "A study of the seismic noise from its long-range correlation properties," J. Geophys. Res. **111**, 1–12 (2006).
[14]P. Gouédard, P. Roux, M. Campillo, and A. Verdel, "Convergence of the two-point correlation function toward the Green's function in the context of a seismic-prospecting data set," Geophysics **73**, V47–V53 (2008).
[15]R. Weaver, B. Froment, and M. Campillo, "On the correlation of non-isotropically distributed ballistic scalar diffuse waves," J. Acoust. Soc. Am. **126**, 1817–1826 (2009).
[16]H. Douma and R. Snieder, "Correcting for bias due to noise in coda wave interferometry," Geophys. J. Int. **164**, 99–108 (2006).
[17]A. Curtis and D. Halliday, "Directional balancing for seismic and general wavefield interferometry," Geophysics **75**, SA1–SA14 (2010).
[18]A. Bakulin and R. Calvert, "The virtual source method: Theory and case study," Geophysics **71(4)**, SI139–SI150 (2006).
[19]K. Mehta, A. Bakulin, J. Sheiman, R. Calvert, and R. Snieder, "Improving the virtual source method by wavefield separation," Geophysics **72**, V79 (2007).
[20]K. Wapenaar, J. van der Neut, and E. Ruigrok, "Passive seismic interferometry by multidimensional deconvolution," Geophysics **73**, A51 (2008).
[21]L. Stehly, M. Campillo, B. Froment, and R.L. Weaver, "Reconstructing Green's function by correlation of the coda of the correlation C3 of ambient seismic noise," J. Geophys. Res. **113**, B11306 (2008).
[22]M. Tanter, J.-L. Thomas, and M. Fink, "Time reversal and the inverse filter," J. Acoust. Soc. Am. **108**, 223–234 (2000).
[23]M. Fink, "Time reversed acoustics," Phys. Today **50(3)**, 34–40 (1997).
[24]A. Derode, E. Larose, M. Campillo, and M. Fink, "How to estimate the Green's function of a heterogeneous medium between two passive sensors ? Application to acoustic wave," Appl. Phys. Lett. **83**, 3055 (2003).
[25]A. Derode, E. Larose, M. Tanter, J. de Rosny, A. Tourin, M. Campillo, and M. Fink, "Recovering the Green's function from field-field correlations in an open scattering medium," J. Acoust. Soc. Am. **113**, 2973–2976 (2003).
[26]M. Tanter, J. F. Aubry, J. Gerber, J. L. Thomas, and M. Fink, "Optimal focusing by spatiotemporal inverse filter. I. Basic principles," J. Acoust. Soc. Am. **110**, 37–47 (2001).
[27]J. F. Aubry, M. Tanter, M. Pernot, J.L. Thomas and M. Fink, "Experimental demonstration of noninvasive transskull adaptive focusing based on prior computed tomography scans," J. Acoust. Soc. Am. **113**, 84–93 (2003).
[28]F. Vignon, J. F. Aubry, M. Tanter, A. Margoum, and M. Fink, "Adaptive focusing for transcranial ultrasound imaging using dual arrays," J. Acoust. Soc. Am. **120**, 2737–2745 (2006).
[29]S. Yon, M. Tanter, and M. Fink, "Sound focusing in rooms. II. The spatio-temporal inverse filter," J. Acoust. Soc. Am. **114**, 3044–3052 (2003).
[30]G. C. Herman and C. Perkins, "Predictive removal of scattered noise," Geophysics **71**, V41–V49 (2006).